Summer 8-4-2023

Development of Air-Jetting System for Bioprinting of Alginate Micro-Droplets

Nathan Lingenfelter

DEVELOPMENT OF AIR-JETTING SYSTEM FOR BIOPRINTING OF ALGINATE MICRO-DROPLETS

A Thesis

Submitted to Duquesne University

Duquesne University

In partial fulfillment of the requirements for

the degree of Master of Science

By

Nathan Lingenfelter

August 2023

DEVELOPMENT OF AIR-JETTING SYSTEM FOR BIOPRINTING OF ALGINATE MICRO-DROPLETS

By

Nathan Lingenfelter

Approved March 22, 2023

Dr. Bin Yang Assistant Professor of Biomedical Engineering (Committee Chair)	Dr. Kimberly Williams Associate Professor of Biomedical Engineering (Committee Member)
Dr. John A. Viator Professor and Chair of Engineering (Committee Member)	Dr. Ipsita Banerjee Associate Professor of Chemical Engineering, University of Pittsburgh (Committee Member)
Dr. Fevzi Akinci Professor and Dean, Rangos School of Health Sciences	Dr. John A. Viator Chair, Department of Engineering Professor of Biomedical Engineering

ABSTRACT

DEVELOPMENT OF AIR-JETTING SYSTEM FOR BIOPRINTING OF ALGINATE MICRO-DROPLETS

By

Nathan Lingenfelter

August 2023

Thesis supervised by Dr. Bin Yang and Dr. Kimberly Williams,

Transplantation of organoids has been demonstrated to be a promising cure to many diseases including Type-1 diabetes. However, achieving consistent and robust derivations of mature organoids from human pluripotent stem cells (hPSCs) is challenging. Cellular mechano-transduction, where mechanical stimuli is sensed and converted to biochemical signaling, has been proposed to overcome this challenge. This pathway relies on encapsulating hPSCs in a small volume of a biomaterial such as alginate, which has been widely used as cell encapsulation materials due to its biocompatibility and selective permeability. In this project, we focused on developing an air-jetting based technique to generate small and consistent spherical alginate droplets in the range of 300 to 500 μm. This can later be used for cell encapsulation and 3D-cell culturing via activation of the mechano-transduction pathway. We developed a custom

alginate droplet generation system by integrating a syringe pump system with a 3D-printed air-jetting adapter. We conducted comprehensive studies to investigate and validate the design and configuration of this system, as well as parameters for droplet generation. Throughout the study, we optimized and developed a working protocol that ensures repeatable and consistent generation of alginate droplet in the targeted size range. The newly developed technique for generating alginate droplets will be incorporated into existing research of biomanufacturing organoids and provide insights for scale-up methods of production.

ACKNOWLEDGEMENT

I would like to express my deepest appreciation to Dr. Bin Yang and Dr. Kimberly Williams for their advice and guidance while completing this project. I would also like to acknowledge members of the Yang Lab including Mirabella Stump, Skylar Wrubleski, and Burton Carbino for their help. Finally, this endeavor would also not have been possible without Dr. Ipsita Banerjee and Miranda Poklar at the University of Pittsburgh, who generously provided their knowledge and expertise.

TABLE OF CONTENTS

Page

LIST OF FIGURES

Page

LIST OF ABBREVIATIONS

hiPSCs – human induced pluripotent stem cells

hPSCs – human pluripotent stem cells

FDM – Fused Deposition Modeling

PLA – Polylactic Acid

PSI – Pounds per Square Inch

w/v – weight by volume

M – Molar

diH_2O – deionized water

rpm – revolutions per minute

mM – millimolar

G – gauge

Chapter 1 Introduction

1.1. Introduction

In recent years, hydrogel beads have emerged as one of the most used platforms for 3D cell cultures [1]. This is due to their biocompatibility, ease of modulation, and mechanical properties that closely mimic natural tissue [2]. The aqueous environment of hydrogels can provide a protective housing for their cargo, such as cells or fragile drugs. Hydrogels also possess a 3D-porous network with semi-permeability that facilitates the transport of nutrients to and from encapsulated cells, while selectively blocking immune response cells and preventing host immune response [3]. Due to these physiochemical properties and the ease of use, 3D hydrogel cell cultures are used to study a wide range of applications such as cancer research, cell signaling pathways, and drug screening [4]. Hydrogel droplets, such as alginate droplets, are also being investigated as 3D cell culture for organoid development and transplantation [4]. Transplantation of organoids has been demonstrated to be a promising cure to many diseases including Type-1 diabetes [3]. However, achieving consistent and robust derivations of mature organoids from human pluripotent stem cells (hPSCs) is challenging.

Utilization of the cellular mechano-transduction pathway has been proposed to overcome this challenge [5]. During this process, cells sense and respond to external mechanical forces. This happens by the activation of mechanosensors on the cell membrane [6]. Once these sensors are activated, they trigger a transduction of biochemical signals within the cell and activate certain intracellular cell signaling pathways. These cell signals can then influence cytoskeleton and gene expression changes [7]. This is particularly important during differentiation, as cells are changing

shape and function. Encapsulating hPSCs in a small volume of a biomaterial such as alginate may better utilize this pathway and promote differentiation and viable organoid formation.

1.2. Role of Alginate Droplets in Cell Encapsulation and Transplantation

Alginate, a natural polysaccharide derived from brown seaweed and algae, has the ability to form a hydrogel under cell friendly conditions and is an ideal candidate as an encapsulation material for cells [8]. Alginate also resembles the natural extracellular matrix, making it a great option for 3D cell cultures. Alginate has been used as a prime candidate for encapsulation of pancreatic islet cells aiming for transplantation as a possible cure for Type 1 diabetes [9]. Patients with this type of diabetes cannot naturally produce insulin, as the immune system recognizes the cells responsible as foreign and eliminates them [3]. By introducing insulin-producing cells that the body does not eliminate, the patient can then produce insulin naturally [3]. The semi-permeable barrier created by the alginate droplet is ideal for this application because insulin and nutrients vital to cell survival are allowed to freely travel in and out of the droplets, while the host immune system is prevented from eliminating the cells. This has been attempted with some success using a chemically modified alginate derivative and achieving viable islet transplantation for 4 months with no immunosuppression [3].

1.3. Existing Alginate Droplet Generation Techniques

Several techniques currently exist to encapsulate different biological cargos in alginate droplets. All methods involve preparation of bioink by mixing the desired amount of cells or cargo with an alginate solution [10]. Alginate droplets are then generated using various techniques into a cationic crosslinking agent, such as calcium

chloride, where droplets are fully crosslinked [11]. Crosslinking the alginate droplets allows them to retain their shape and gives them more rigid mechanical properties [12].

The simplest alginate encapsulation method is to make the droplets by hand. In this technique, the cell-alginate solution is added dropwise to the crosslinking solution from a specific height, via a syringe with an attached needle [13]. This encapsulation technique is effective for producing larger droplets (~1mm). However, the droplet size with manual generation does not satisfy the size requirement for activating the mechano-transduction pathway.

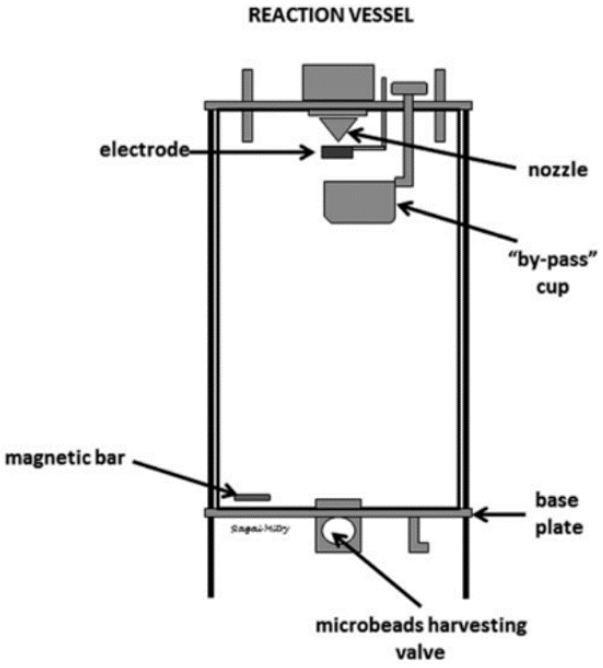

Figure 1. Electrostatic droplet generation setup. Image adapted from Mitry et al. [14].

Several other techniques have been developed to gain more control over droplet shape and size. Among them is electrostatic droplet generation. This method utilizes electrostatic forces to create and control the formation of droplets [14]. In this setup, an electrode near the nozzle applies an electric potential to the encapsulation material (Figure 1). This forms a liquid jet that is influenced by surrounding electrostatic forces,

which induces a charge on the surface and breaks the jet up into a stream of individual droplets. This occurs because the electrostatic forces overcome the surface tension of the alginate solution. These droplets then fall to a grounded collection solution, where they are crosslinked [15]. The size of the resultant droplets can be adjusted by varying certain parameters of the setup such as alginate flow rate, applied voltage, and distance between droplet formation and the collection solution.

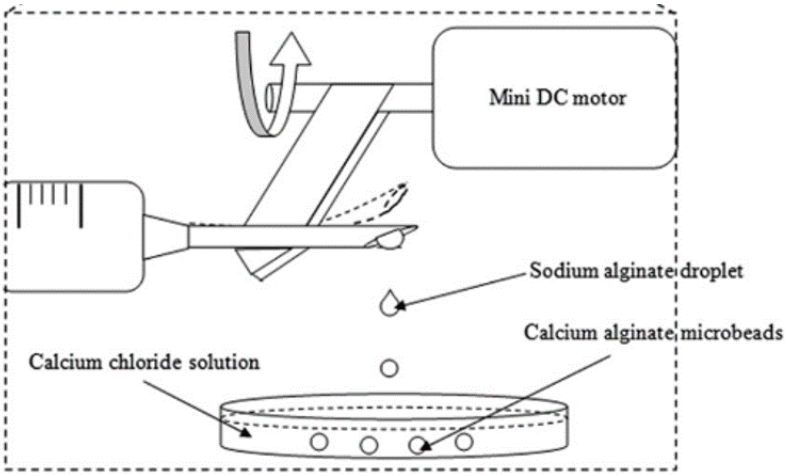

Figure 2. Flicking method droplet generation setup. Image adapted from Wong et al. [16].

A more mechanical example is the flicking method developed by Wong et al. [16]. This method utilizes a syringe pump and a gear motor that spins a plastic tie around and manually contacts the needle, causing the alginate droplet to separate (Figure 2). This method is a simple, low-cost droplet generation technique. However, it may not be suitable for applications requiring precise control over droplet size and shape.

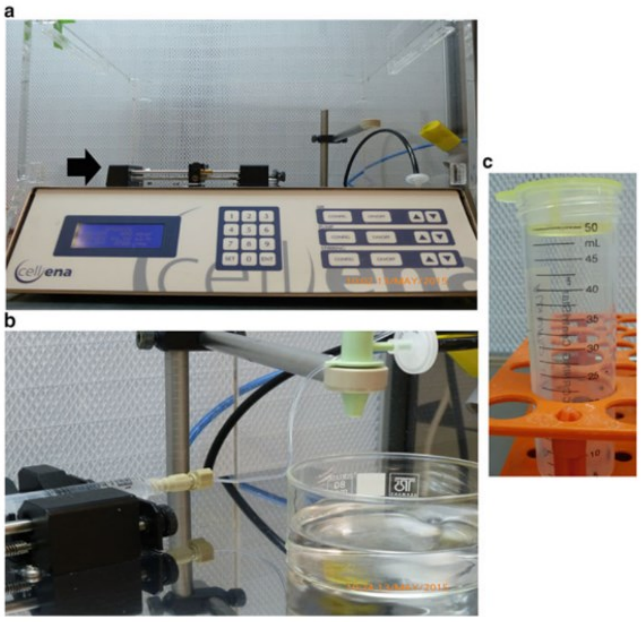

Figure 3. Nebulizer droplet generation setup. (a) Nebulizer with black arrow indicating the peristatic pump. (b) Encapsulation system setup. (c) Solution filtering setup. Image adapted from Ciriza et al. [17].

Another known method is to use a nebulizer to convert alginate solution into a focused stream of mist that can be captured as droplets [17]. In this method, the alginate solution is supplied to a nebulizer device, which contains a mechanism for atomizing the liquid (Figure 3). There are several different mechanisms with which this can be achieved, and some may be more suitable than others for cell survival, depending on the application. The nebulizer breaks up the solution into small droplets which are then directed towards a collection chamber. The size of the droplets produced with this method can be influenced by several factors including solution properties, nebulizer design, solution flow rate, and applied energy.

Microfluidic systems are yet another viable option to produce alginate droplets. In this method, two liquids (an aqueous and an organic) flow in the same chamber and meet at a junction where they form droplets. The size of these droplets is dependent upon the liquid properties, flow rates, and geometric components of the setup [10]. Lastly, air can

be used in several ways to produce alginate droplets [10]. The jet cutting method uses air to “cut” a continuous stream of liquid alginate at the proper interval to achieve the desired droplet size. With the air-jetting technique, air flows around the needle and is used to separate the alginate droplets from the tip of the needle at the desired size as they are extruded [18].

1.4. Air-Jetting Based Droplet Generation

Air-jetting based droplet generation, among all available techniques, seems of particular interest due to several advantages. The design and fabrication process for an air-jet attachment is relatively simple and low-cost compared to other methods. This allows us to produce a working air-jet device using 3D design and printing techniques that can be quickly implemented into our system and modified as necessary [19]. Similar air-jet techniques have also been used in other studies that achieved consistent quality performance [18, 20]. Moreover, minimal efforts are needed to incorporate air-jetting based droplet generation into existing research and workflow. Lastly, the simplicity and reproducibility of this technique also adds scale-up potential from a biomanufacturing standpoint.

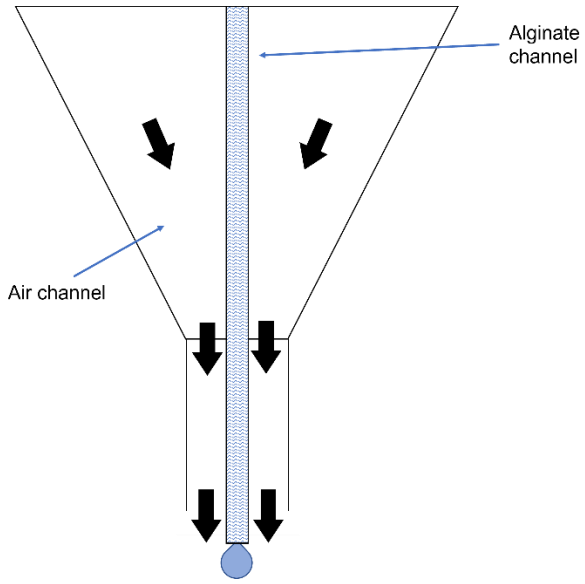

Figure 4. This graphic shows a schematic example of how air-jetting works. The white regions represent the air channel inside the air jet attachment. The blue patterned region represents the channel containing alginate, typically a needle. Black arrows indicate direction of air flow.

Air-jetting works by introducing pressurized air flow around the newly generated droplet at the tip of the needle, which can be achieved by an air-jetting adapter [21]. A visual representation of this arrangement is shown in Figure 4. The innermost channel, which is a syringe and needle in our case, contains the alginate solution and is connected to the extrusion mechanism for steady output of alginate. Surrounding this channel is another, larger channel for air flow that is connected to a source of pressurized air. As alginate flows through the center, it forms droplets at the end of the needle that eventually become heavy enough to separate from the needle and fall to the collection liquid. By surrounding this with a constant flow of air, the air will cause the droplets to separate from the needle at a smaller size than they would naturally. The size of droplets is collectively determined by many factors, including the needle size, the air flow rate and extrusion rate of alginate solution.

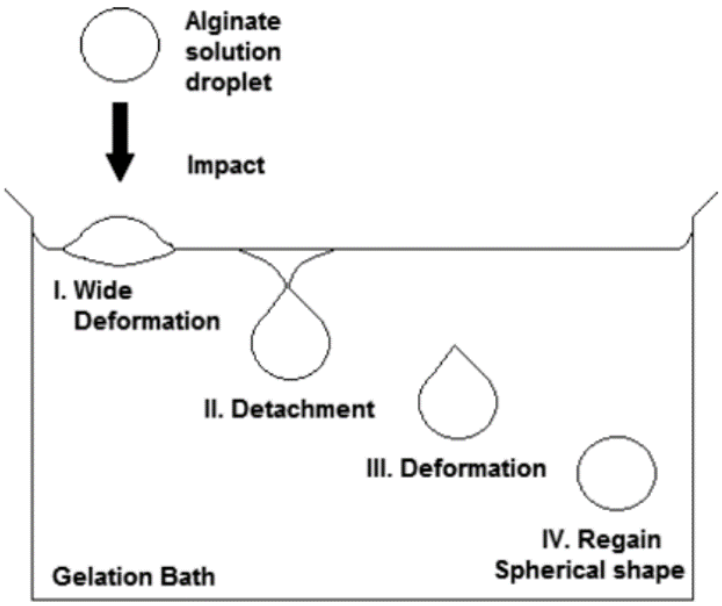

Figure 5. Alginate droplet impact and deformation upon entry into the collection bath. Image adapted from Lee et al. [22]

The final droplet shape is also reliant on how the falling droplets act as they are collected in the crosslinking bath. Previous studies have shown that the impact force of the alginate droplet hitting the surface of the crosslinking solution plays a major role in determining the shape of the formed droplets [22]. Figure 5 shows an illustration of what typically happens to an alginate droplet as it interacts with the collection liquid. The falling droplet will experience the most deformation as it first hits the gelation bath surface. In the ideal case, it will then detach from the surface and become totally submerged in the solution. This detachment causes deformation; however, the droplet will regain its shape as it begins to settle and crosslink. The ability of the droplets to regain their spherical shape relies on the properties of the alginate solution and the height of droplet formation above the gelation bath (or the velocity of the beads as they impact the solution).

1.5. Goal of This Study

The goal of this project is to develop a robust approach based on air-getting technique to generate alginate droplets in the range of 300 to 500 μm. To achieve this goal, we identified two objectives. The first objective focused on developing and validating a droplet generation system by integrating a syringe pump with a 3D printed air-jetting adapter. In the second objective, we focused on optimizing the parameters for generating consistent alginate droplets in the targeted range. The air-jetting based droplets generation technique will be integrated into organoid biomanufacturing research.

Chapter 2 Development of Air-Jetting Based Bioprinting System

2.1. Introduction

The two most important components for an air-jet system are a liquid extrusion system and an air flow system that is used in conjunction with the liquid component. Previous research has demonstrated that both alginate channel and air channel can be 3D printed to form a single and integrated air-jet attachment [20]. In this work, we chose to use a syringe and needle for the alginate delivery, as needles provide smaller and more consistent inner diameters than 3D printing would allow, which is crucial to generating droplets with small and consistent diameters. Changing the parameters of other attachment components, such as air channel inner diameter and shape, can also impact how the air flowing through it acts on the needle. This chapter focuses on the design alterations and testing that took place to obtain the final, optimized design.

2.2. Air-Jetting Attachment Design and Fabrication

The 3D printed air-jet attachment used in this project was designed using Fusion360 (Autodesk, San Rafael, CA) and underwent multiple design iterations before a viable model was achieved. The air-jet attachment design features an air inlet, an inner chamber to stabilize the air, and a channel around the needle to provide a consistent air flow to separate the droplets from the needle (Figure 6). The overall body shape of the attachment remained mostly unchanged from the first iteration (Figure 7A) to the last (Figure 7C). However, the details of these individual components were optimized and finalized through testing.

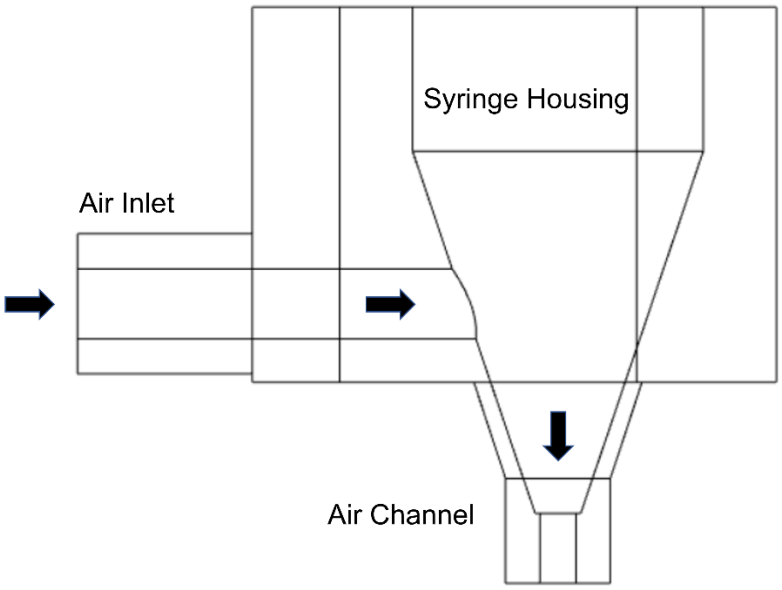

Figure 6. A wireframe view of the air-jet attachment with the main components labeled. Black arrows indicate direction of air flow.

The cylindrical protrusion on the bottom of the air-jet attachment is where the air exits around the needle and is what we refer to as the air channel. Initially, the air channel was a tapered cone-like shape (Figure 7A). The main purpose of this shape is to smoothly reduce the diameter of the air channel from a large diameter the size of the syringe, down to a smaller diameter that surrounds the needle appropriately. This shape was later changed to a tapered design within the main body of the attachment, but with a straight cylinder that protrudes from the body (Figure 7B). This change was made to promote steady air flow around the end of the needle. However, this design was abandoned as the printing of the hard corner where the cylinder meets the main body was problematic. These two design concepts were combined in the final form of the air channel design. The cone structure was beneficial for printing purposes and for the inner structure of the attachment. By including a straight cylinder on the end of the protruding cone (Figure

7C), we can preserve those facets while utilizing the simpler air flow dynamics of a straight tube.

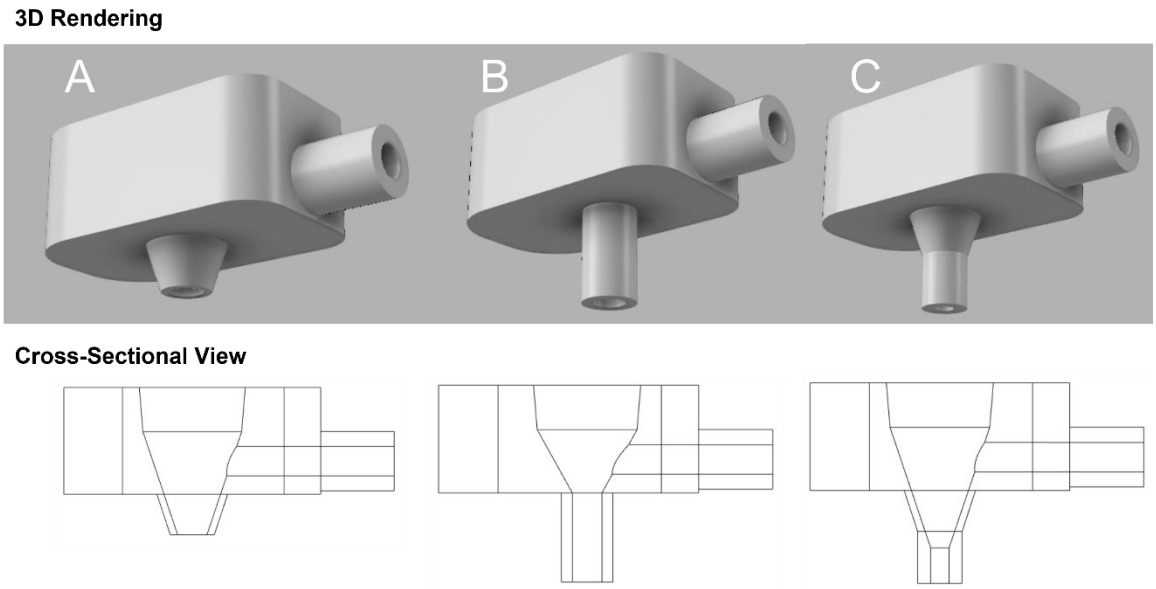

Figure 7. Several different iterations of the design of the air-jet attachment, with the corresponding wireframe views below each one. (A) The initial design with a short, tapered air channel that features a wider inner diameter. The air channel length is much shorter than the needle when inserted (B) A design iteration with a long, straight air channel that extends to the end of the needle. (C) The final air channel shape, a tapered section with a straight extension that is slightly shorter than the end of the needle.

Once the shape of the air channel was established, the inner diameter and length could be examined through experimentation. In early designs, the syringe needle would extend well past the end of the air channel with a large inner diameter. This was not the best way to maximize air pressure on the forming droplets, however. Making the diameter smaller allowed for greater air pressure to build up and exit the channel, reducing the amount of air flow required to force droplets off the needle. On the other hand, an inner diameter of less than 1mm puts heavy reliance on the accuracy of the 3D printer, makes centering the needle for straight printing a challenge, and could cause issues with pressure build-up at other points of the printing setup.

The length of the air channel also plays a role in how effective the droplet printing process is. There are 3 overarching positions for the needle with respect to the end of the

air channel: the needle tip could be outside the air channel, in line with the end of the air channel, or inside the air channel. While having the tip of the needle inside or in line with the end of the air channel would theoretically expose it to the most concentrated air flow, this presented issues of droplets hitting the inner wall. Taking both of these factors into consideration simultaneously, it was determined that an inner diameter of 2mm with the air channel slightly shorter than the needle was the ideal configuration. A study in which the exact distance that the needle should be past the air channel is discussed in section 3.4.2.

Early iterations of the attachment were printed using a MakerBot Replicator+ (MakerBot, New York City, NY) which utilizes fused deposition modeling (FDM) to print prototypes using polylactide (PLA). This method of printing served a purpose for early designs but was susceptible to leaks and small-scale flaws in finished models. We switched to a Formlabs Form 3+ stereolithography printer (Formlabs, Somerville, MA) for the later iterations of the design. Stereolithography, or resin printing, uses UV light to cure the liquid resin in place on the print bed surface. This method allows for much higher accuracy and resolution of prints, eliminating many of the issues of printing with FDM. This is especially important for the design of where the syringe is inserted, as that hole is designed to be very close to the outer diameter of the syringe. This way, the syringe can be inserted with some force and an air-tight seal will be formed between the attachment and syringe. This seal is checked periodically as the attachment undergoes normal wear and tear and this configuration should be optimized in the future.

2.3. Alginate Extrusion Method

The initial proposal for this work included retrofitting a commercial 3D bioprinter (Allevi 1, Allevi Inc., Philadelphia, PA) with the air-jetting attachment to enable air-jetting capabilities (Figure 8). One of the early prototypes is shown in Figure 8. This air-jetting attachment uses pressurized air from an external air compressor as its source of power for extruding materials.

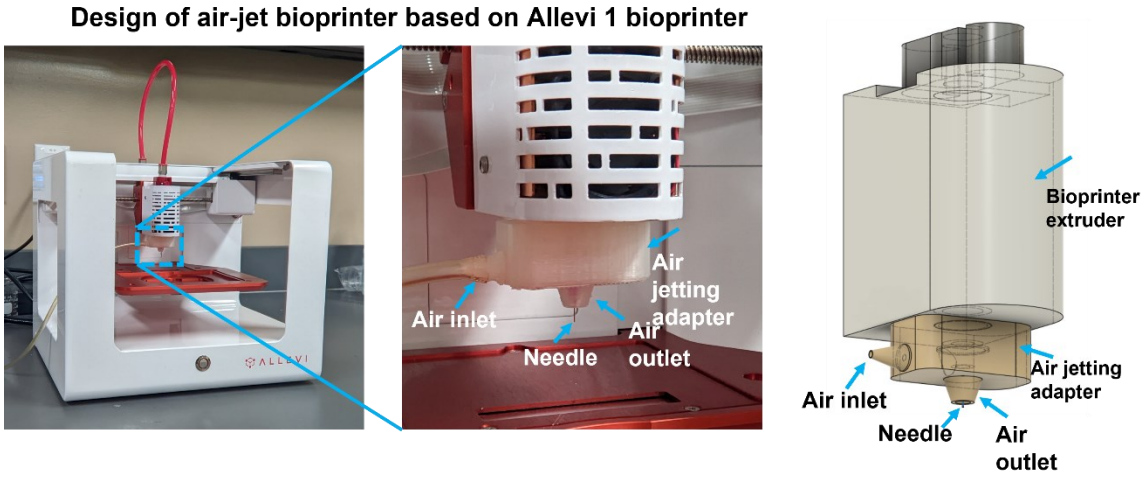

Figure 8. The initial printing setup using an Allevi 1 bioprinter. (Left) The Allevi bioprinter with fitted air-jet attachment. (Middle) Magnified view of the air-jet attachment connected to the bioprinter extrusion housing. (Right) 3D rendering of the main components of the printing setup.

However, the Allevi 1 bioprinter has several limitations that are relevant for this research. First, the Allevi 1 can accommodate pressures between 3-100 PSI and it was discovered through experimentation that this pneumatic extrusion method becomes unstable at very low extrusion rates, as our printing typically occurred in the lowest part of this range of pressures. The result of this inconsistent extrusion rate is resultant droplets with varying size, shown in Figure 9. The Allevi 1 also has an extruder that can move laterally but is fixed vertically. The print bed moves up and down to bring the extruder to the print surface. This means that there is a limitation to the distance between the needle and the crosslinking solution that the droplets fall into. Our testing suggested that we need roughly 14cm of distance between the crosslinking bath and the extrusion

needle to achieve a spherical shape of droplets, which cannot be accommodated by the Allevi 1. The extruder housing of the Allevi 1 bioprinter also contains a fan and vents for temperature control. This means that the housing is not airtight and some air that is introduced for air jetting is lost.

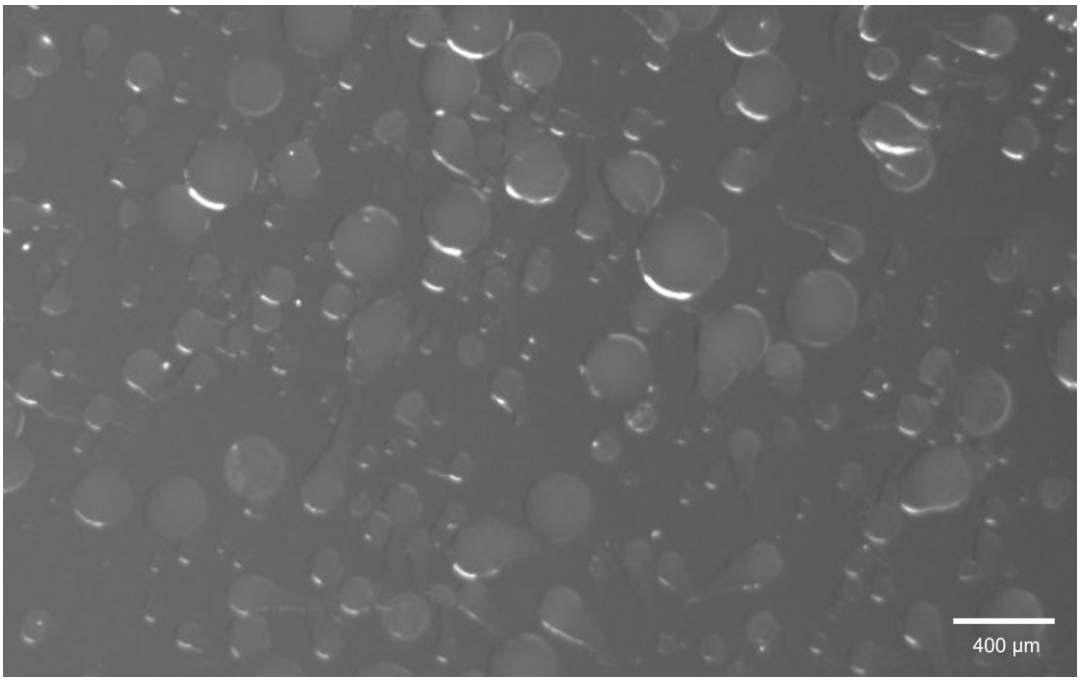

Figure 9. Image of droplets produced using the Allevi 1 bioprinter at 4 PSI and with an air flow rate of 3.5 L/min. These droplets exhibit a large variation in size due to inconsistent extrusion.

Due to these limitations, a decision was made to replace the 3D bioprinter with a syringe pump system for generating alginate droplets (Figure 10). Mechanical extrusion provides better control and more consistency with regards to extrusion flow rate. This change also allows for more variability in changing droplet fall distance and an airtight seal between syringe and attachment.

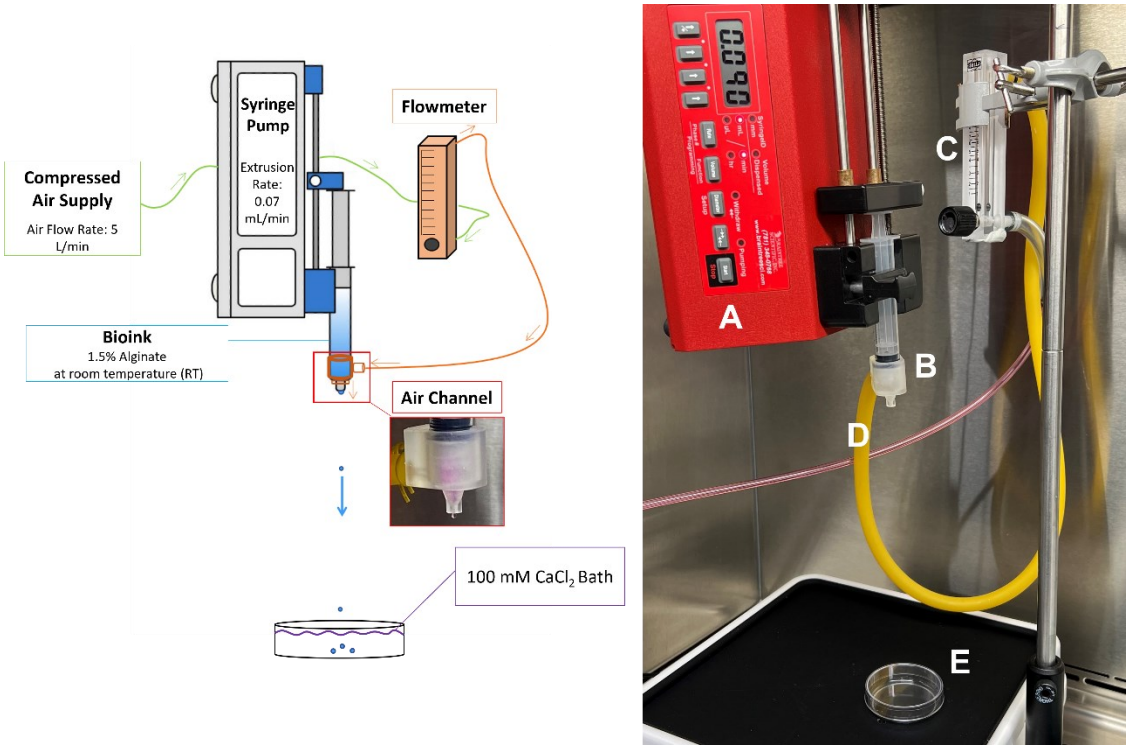

Figure 10. The final syringe pump printing setup. (A) The syringe pump unit. (B) A 10mL syringe with a 30G needle and the air-jet attachment connected at the lower end. (C) Flowmeter to measure air flow rate. (D) Rubber tubing that supplies air to the attachment. (E) Calcium chloride crosslinking solution positioned below the extruding setup at a viable distance.

2.4. Conclusion

By completing this study, we were able to achieve a working design that is robust and produces satisfactory results. Our air-jet attachment can be easily fabricated with a resin 3D printer, and it can be modified to fit individual needs. A future direction of this work is to integrate a syringe pump system with the main frame of the Allevi 1 to achieve optimal extrusion as well as 3D printing positioning/printing capabilities.

Chapter 3 Comprehensive Studies for Optimizing the Shape and Size of Alginate Droplets

3.1. Reagent Preparation

The desired concentration (w/v) of alginate solution was obtained by dissolving the appropriate amount of alginate powder (W201502, Sigma-Aldrich, Merck KGaA, Darmstadt, Germany) in diH_2O that was dispensed from a water deionization system (Elga Flex 3, Woodrige, IL). The beaker containing water, alginate powder, and a stir bar was placed on a hot plate (VWR International, Radnor, PA) at 60°C and a glass cover was placed on top to minimize evaporation. The solution was allowed to spin at 500rpm for 40 minutes. Once stirring is complete, the glass cover is removed, any condensation that may have formed from heating is recovered, and the solution is filtered using 0.22µm sterile filters (Millipore Sigma, Merck KGaA, Darmstadt, Germany). The standard alginate concentration used in this study was 1.5% and this was the concentration used for all tests, unless otherwise stated.

Calcium chloride solutions as the crosslinking agent were also prepared for this study. The desired concentration (M) was obtained by dissolving the appropriate amount of solid CaCl2 (C1016-100G, Sigma Aldrich) in diH2O that was dispensed from a water deionization system (Elga Flex 3, Woodrige, IL). The solution was stirred at 400rpm and solid calcium chloride was added periodically until totally dissolved. The dissolved solution was then filtered using 0.22µm sterile filters (Millipore Sigma, Merck KGaA, Darmstadt, Germany). The concentration of CaCl2 used in this study was 100mM unless otherwise stated.

3.2. General Printing Process

The following is a detailed procedure for the air-jet printing process. First, the alginate solution is allowed to reach room temperature from its cooled storage temperature. Prepared alginate solution is then loaded into a 10mL syringe (14-955-459, Fisher Scientific, Hampton, NH) and the syringe is fitted with a 0.25-inch, 30G needle (PT30-0.25, Allevi Inc., Philadelphia, PA). Bioink solution is pushed through the needle to ensure there is proper flow with no clogs. Once filled, the syringe is firmly pressed into the 3D printed air-jet attachment until the needle is in the middle of the air channel and with a desired exposed needle length. The seal between the attachment and syringe is checked for air leaks as needed. The syringe with attachment secured is then placed into the syringe pump (BS-300, Braintree Scientific, Braintree, MA) for printing. The air-jet attachment is also connected via rubber tubing to an air compressor (PC1010, Senco, Cincinnati, OH). This connection runs through a flowmeter (LZQ-7, SHLLJ, Zhejiang, China) to accurately measure the air flow rate through the attachment. A collection Petri dish is filled with 10 mL of calcium chloride solution and placed under the syringe/attachment nozzle. The height of the syringe over the calcium chloride solution is specified and can be adjusted.

At this point, the syringe pump is turned on and given time to ensure extrusion is occurring and normal. Once that is done, the pressurized air is slowly turned on, allowing time for the flow to stabilize and for any liquid buildup on the end of the attachment to be wiped away. When the air flow is stable and droplets are forming, the lid of the collection Petri dish is removed, and collection can begin. Normal collection time is one minute. When collection has completed, the lid is replaced, and all flow can be turned off.

3.3. Alginate Droplet Imaging and Analysis

Alginate droplets were collected in individual Petri dishes (Fisher 60 x 15mm stackable Petri dish, Pittsburgh, PA) that could then be moved to an inverted 4X microscope (AmScope, Irvine, CA) with an attached camera (6MP USB 3.0 Cooled Color CCD Camera, AmScope, Irvine, CA) for viewing and imaging. Images were captured using the camera and image acquisition software from AmScope.

```
clc
clear all
close all
%designate folder that contains images to be analyzed
folder='C:\Users\nathl\Desktop\Yang Lab\Droplet Images\12.05 Grid\';
%load multiple droplet images of the same sample
img1=rgb2gray(imread([folder 'N1_0.07min_5.jpg']));
img2=rgb2gray(imread([folder 'N2_0.07min_5.jpg']));
img3=rgb2gray(imread([folder 'N3_0.07min_5.jpg']));

img=cat(2,img1,img2,img3); %combine multiple images to a single one

%display images, draw line across 1 droplet to estimate diameter of group
figure
imshow(img)
d = drawline; %create draggable line
pos = d.Position;
diffPos = diff(pos);
D = hypot(diffPos(1),diffPos(2));

%% show good detections
margin=0.2; %indicates range of acceptance on either side of the estimated diameter, in this case 20%
[centers, radii, metric] = imfindcircles(img,[round(D/2*(1-margin)) round(D/2*(1+margin))],'Sensitivity', 0.97);
idx_good=find(metric>0.08); %denotes "good" circle acceptance
centers_good=centers(idx_good,:);
radii_good=radii(idx_good);
figure
imshow(img)
viscircles(centers_good, radii_good, 'EdgeColor','b');
%% show all detections
%show detected circles before filtering for "good" circles
figure
imshow(img)
viscircles(centers, radii, 'EdgeColor','b');

%% quantification
%radius and diameter calculations
calibrator=1.1; %um/pixel
mean_radius=mean(calibrator*radii_good);
std_radius=std(calibrator*radii_good);
mean_diameter=mean_radius*2
std_diameter=std_radius*2
```

Figure 11. Droplet quantification MATLAB script.

These images were then analyzed for size and shape measurements using ImageJ (NIH, Bethesda, MD) and a custom droplet quantification script via MATLAB (MathWorks, Natick, MA) shown in Figure 11. This script measures the diameters of

droplets from multiple images that fit the size and shape specifications denoted in the second section.

3.3.1. Statistical Analysis

Statistical data was collected on select studies to determine significance in droplet size differences between groups. Statistical analysis was performed using MATLAB. Significant differences were calculated using a t-test (comparing two experimental samples) or a one-way ANOVA (comparing more than two samples) followed by Tukey's test. Tukey's test is a single-step multiple comparison statistical test that is used to find averages of different samples that are significantly different from each other [23]. The data was represented as mean ± SD and a significant difference was considered as $p < 0.05$ unless otherwise stated.

3.4. Parameter Optimization

For cells to thrive and behave as expected the droplets that encapsulate them must possess certain geometric and size qualities. Many parameters of the syringe pump air-jetting system can be adjusted, including extrusion speed and air flow rate, which will affect the size and shape of the generated droplets. Therefore, a series of studies was conducted to study and optimize printing parameters to achieve consistent printing with the desired shape and size.

3.4.1. Extrusion Rate vs Air Flow Rate

The first, and most overarching, of these studies looked at the relationship between the rate at which alginate bioink was extruded from the needle and the flow rate of the air through the air-jet attachment. In general, higher air flow would produce more force at the tip of the needle, forcing droplets off faster and resulting in smaller droplets

(at a steady extrusion rate). Speed at which the droplet falls to the crosslinking solution could also impact the final shape. Higher extrusion rate would indicate that droplets form at the needle tip faster, which would produce larger droplets at the same air flow rate. To determine how these two factors can be optimized for ideal size and shape, a comprehensive study was completed. Two viable ranges for the extrusion rate (0.03, 0.05, 0.07, 0.09, and 0.11 mL/min) and air flow rate (2-6 L/min) were selected based on results from previous experimentation. A total of 25 samples were printed, collected, and imaged with printing parameters covering these entire ranges. Based on our experience in testing, we selected the following printing parameters, which were held constant throughout the experiment: distance between the needle and the calcium chloride bath (13.5 cm), exposed needle length (1 mm), calcium chloride concentration (100 mM), inner diameter of air channel (2 mm). The alginate printing stage of this study was done without dismantling or altering the printing setup to ensure that all outside factors were the same for each sample. The study was also completed twice to show reproducibility of results.

Figure 12 shows one image from each collected sample at each of the parameter combinations. Looking at all the collections at once gives an overall impression of the size and shape trends associated with the varying air flow rate and extrusion rate. As the air flow is increased, the size of the droplets decreases. As the extrusion rate is increased, the effect on size is not as significant. The shape of the droplets also becomes more spherical as air flow rate increases. However, shape may worsen slightly at 6 L/min due to too much force on the droplets. This can result in broken or weak looking droplets. Some droplets also exhibit a flat portion of the surface. This indicates that the droplets

did not fully submerge into the crosslinking solution but instead floated just under the surface. Upon completion of this study and review of the results, we selected a final extrusion rate of 0.07 mL/min and a final air flow rate of 5 L/min. These parameters were then used to complete the remaining studies. With these factors held constant, we were able to further optimize other aspects of our printing procedure.

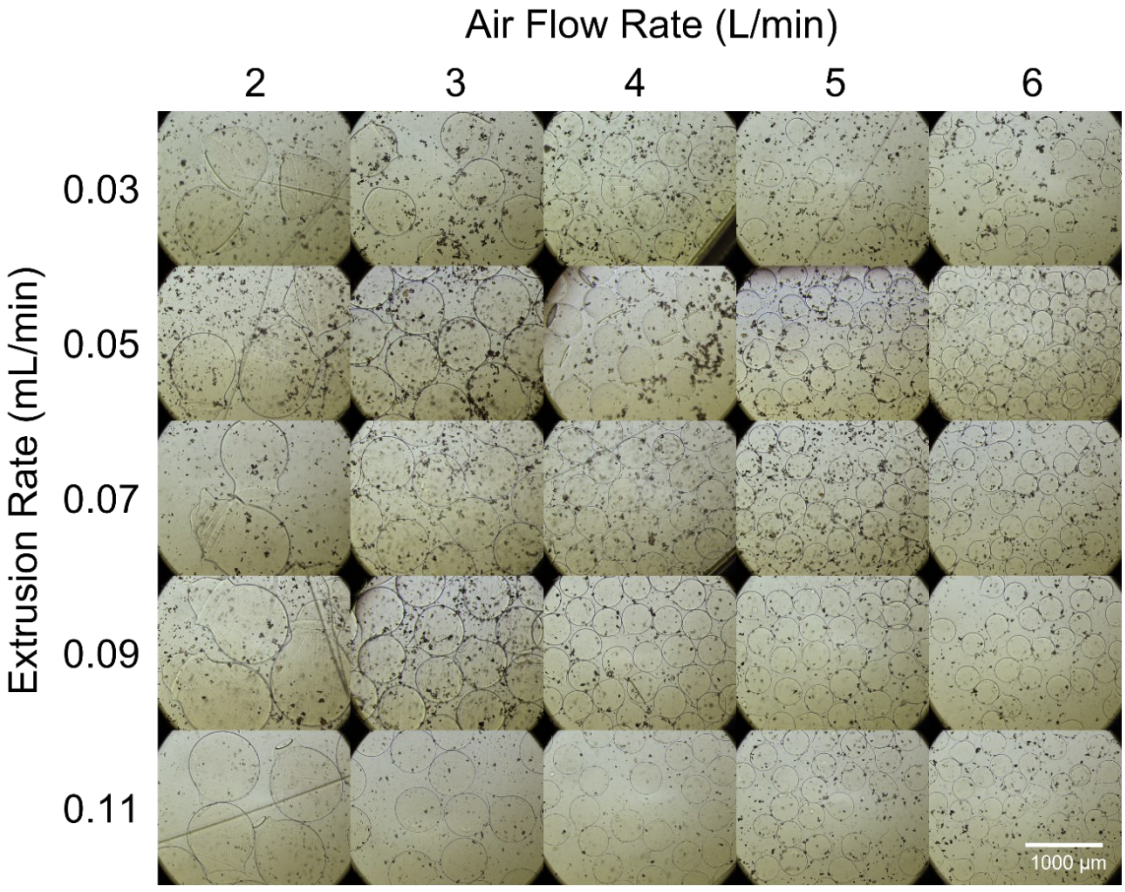

Figure 12. Images from the air flow rate vs. extrusion rate study. These images were selected because they show a representative population of the geometry of the droplets in each sample.

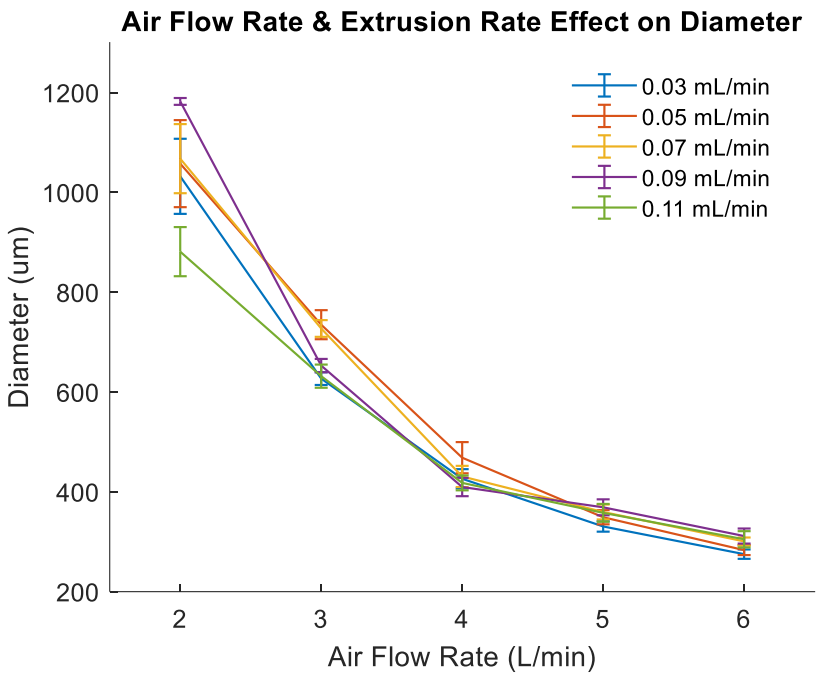

Condition Pairs		Mean Difference	MD Lower	MD Upper	p-value
3 L/min	4 L/min	252.61	266.79	280.97	0
3 L/min	5 L/min	320.65	334.2	347.75	0
3 L/min	6 L/min	378.73	392.28	405.82	0
4 L/min	5 L/min	58.019	67.412	76.806	0
4 L/min	6 L/min	116.09	125.49	134.88	0
5 L/min	6 L/min	49.672	58.074	66.476	1.1473E-36

Figure 13. The influence of air flow rate and extrusion rate on droplet diameter. Experiments were performed at five different extrusion rates, listed in the top right and represented as individual lines on the plot, and five different air flow rates, shown along the x-axis. All experiments were conducted using a 30G needle with identical printing setups. Statistical significance was determined by one-way ANOVA, followed by Tukey's test. The table shows values from Tukey's test conducted on the samples at a constant extrusion rate of 0.07 mL/min. The first two columns indicate the samples being compared. The following three columns show the mean difference followed by its lower and upper limits. The final column displays the *p*-values for each comparison.

Figure 13 shows a graphical representation of the relationship between the droplet size and the air flow rate at different extrusion rates. As the air flow rate increases (increasing values on the x-axis), the size of the droplets is greatly reduced. This occurs with all extrusion rates that were used. Based on the ranges of parameters tested in this experiment, it is evident that the air flow rate had a greater effect on droplet size than extrusion rate.

Figure 13 also shows a table from Tukey's test, that was obtained during the statistical analysis of this section. The table represents analysis of each sample obtained at a constant extrusion rate of 0.07 mL/min. The first two columns indicate the samples being compared, while the last column shows the *p*-value for the pairwise comparison between the groups. Each *p*-value lower than 0.05 denotes a significant difference between the diameter size of the groups being compared. The remainder of the data from this testing can be found in the appendix. Statistical assessment of this data confirmed the hypothesis that with a fixed extrusion rate, droplet sizes will be different at different air flow rates. Because the most consistent results occurred in the lower right section of the air rate vs. extrusion rate grid, samples obtained at an air flow rate of 2 L/min and an extrusion rate of 0.03 mL/min were omitted from this analysis.

3.4.2. Exposed Needle Length

In the alginate droplet printing setup, a syringe with an attached 0.25-inch long 30G needle is inserted into the air-jetting attachment. The needle itself, once fastened onto the syringe, is longer than the channel on the end of the attachment where the pressurized air exits. Changing the positioning of the needle affects how the pressurized air from the air channel acts on the forming droplets. This study focuses on different needle positions and how they will impact the size and shape of the produced droplets. Using the selected parameters of 0.07 mL/min and 5 L/min from the previous study, exposed needle lengths of 0.5mm, 1mm, and 1.5mm were tested. These varied lengths were achieved by pushing the syringe into the air-jet attachment at different depths and then measuring the visible portion of the needle using calipers (500-196-20, Mitutoyo, Aurora, IL). Figure 14 shows the trend of the diameter of alginate droplets as they

correspond to each length. Figure 14 also includes representative images from each of the samples to show the relative geometry of the droplets between collections. As the length of exposed needle increases, droplet size is reduced. However, at an exposed needle length of 1.5mm the droplets begin to take on a less spherical shape. An exposed needle length of 1mm allows for a smaller droplet size than 0.5mm while still maintaining a largely spherical shape.

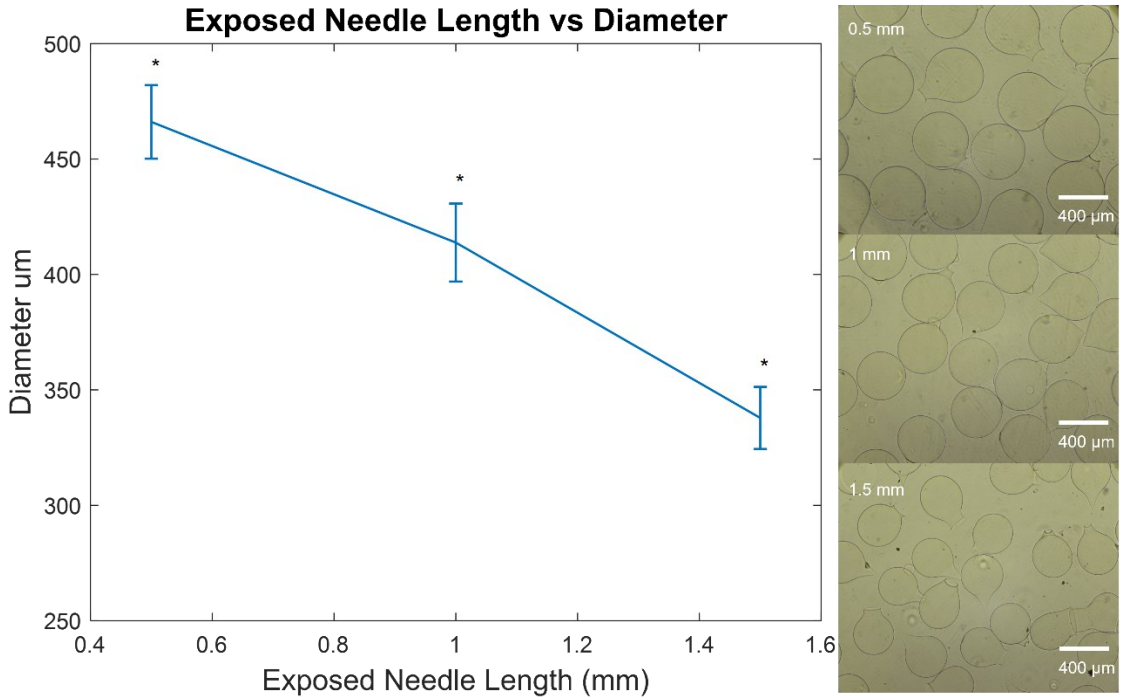

Figure 14. The effect of the exposed needle length on droplet diameter and geometry. The graph on the left shows diameter measurements taken at three different needle lengths (0.5mm, 1mm, 1.5mm). Images on the right are a representation of geometry of each sample at 0.5mm (top), 1mm (middle), and 1.5mm (bottom) of exposed needle. The data is represented as mean ± SD. The significant difference is determined by pairwise t-test. *$p < 0.005$.

3.4.3. Alginate Concentration

The proposed air-jet printing technique works by using pressurized air to "push" droplets of the printed material off the end of the needle at the appropriate time to achieve the desired size. This means that not only are extrusion rate and air flow rate important variables to consider, but the concentration of the bioink is also a crucial component. The numbers chosen for extrusion and air flow rates depend almost entirely on the

concentration of the material and different concentrations could produce different results at the same printing parameters. To test this, a study was performed in which the percentage of alginate in the printed bioink was altered. This experiment used the standard 0.07 mL/min extrusion rate and 5 L/min air flow rate that was used in previous studies. Alginate samples of 1%, 1.5%, and 2% (all dissolved in deionized water) were tested. Figure 15 shows images of the resultant droplets. Droplets of 1% alginate do not appear spherical and possess a very weak and abnormal shape. This is likely because the alginate solution is too weak and possesses physical characteristics closer to that of water. Droplets made with 1.5% alginate appear mostly spherical and a percentage of droplets have small tails. Droplets made with 2% alginate have the most spherical shape of the three concentrations and a smaller percentage of droplets have small tails. For the application of this project, we are limited to alginate concentrations around 1.5%, because the cells that we will be incorporating later do not have a high survival rate at higher alginate concentrations. However, this information could be useful for other studies.

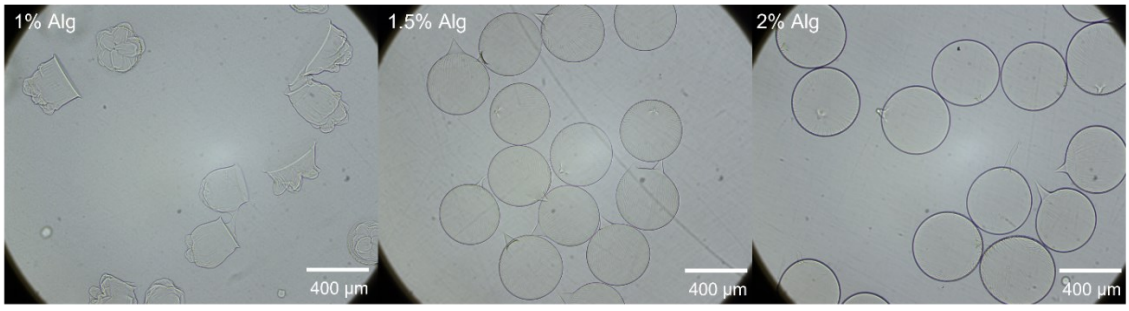

Figure 15. Images of alginate droplets produced at the same conditions with different solutions of alginate. These images show the geometry change with 1% (left), 1.5% (middle), and 2% (right) alginate concentrations.

3.4.4. Crosslinking Agent Concentration

As the alginate droplets are being produced, they fall a specified distance into a solution of calcium chloride, where they are crosslinked. Ideally, a lower concentration of

calcium chloride is preferred to promote cell survival. However, lower concentration calcium chloride slows the crosslinking process, potentially resulting in worse droplet shapes. A study was done to determine how varying the concentration of the CaCl2 solution affected the dynamics of the crosslinking process and final shape of the droplets. Droplets were fabricated using the aforementioned technique at the same parameters, the only difference being the crosslinking solution they fell into. Calcium chloride solutions of 50mM and 100mM were tested. Each sample was allowed to fully crosslink for 8 minutes before they were spun in a centrifuge to remove calcium chloride and isolate droplets. Figure 16 shows images of the resulting droplets. The shape of the droplets in 100mM calcium chloride appear to be much more spherical than the 50mM samples. Droplets in the weaker solution exhibited a bell-shaped feature at one end of the droplet that was not present in the stronger calcium chloride solution. We speculate that the droplets complete the crosslinking process at the surface of the $CaCl_2$, rather than fully submerged, which results in flat surfaces.

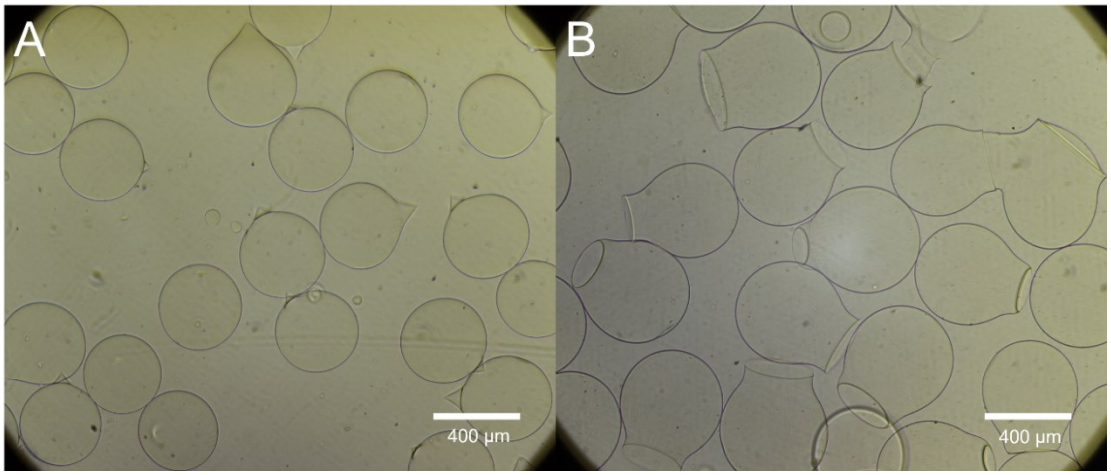

Figure 16. These images show the geometric differences between crosslinking alginate droplets produced at the same parameters in 100mM (A) and 50mM (B) $CaCl_2$.

Chapter 4 Discussion and Conclusion

The results of each parameter study allowed us to optimize the printing setup piece by piece. Some interesting trends were also discovered along the way. During the extrusion vs air flow study, we chose a range of 2-6 L/min for air flow and 0.03-0.11 mL/min for extrusion rate. The results of this study suggest that droplet size depends mostly on air flow rate, rather than the extrusion rate. This could be due to the relatively small range of extrusion rates that were tested. For example, if the extrusion rate were changed more dramatically between each sample set, the results may be different. However, if the extrusion rate were too high, it would take a very large amount of force from the air flow to separate the beads from the tip at an acceptably small size. This excess force could affect the geometry of the droplets, potentially causing them to fracture upon impact or in the air.

Our presented alginate droplet fabrication setup possesses certain advantages and disadvantages. The relatively simple production setup makes fabricating alginate droplets with this technique fairly easy. The attachment itself is cost effective to produce and can be printed with a resin 3D printer. The main advantage of this setup is its adaptability. Our technique can be adjusted to produce droplets for many different alginate concentrations just by altering a few parameters. It can also be modified to produce droplets in a wide range of sizes. In cases where changes to bioink or desired droplet sizes are small, these modifications may be possible by adjusting only one parameter (i.e., air flow rate). The air-jet attachment itself can be used with any extruding mechanism that involves a syringe and can even be modulated to support other extrusion methods such as a bioprinter.

This adaptability does come with certain downsides, however. Since every recreation of this setup may not be identical, it may take several attempts to identify and optimize the appropriate printing parameters. A short trial-and-error type exploration will likely need to be conducted if any component of the setup is changed.

In this study, we developed a robust alginate droplet generation technique that can produce uniform, spherical droplets within the target size range (250 – 400 μm). This technique will allow us to fully control the shape and size of droplets, which is critical for hiPSC encapsulation in order to precisely control the number of cells per droplet. This control also helps to achieve the necessary droplet size to utilize the mechano-transduction pathway during cell differentiation. These are both vital components to the creation of viable organoids.

This work began by designing an effective device for enabling air-jetting in our printing setup. To design an optimal air-jet attachment, many of the components of the attachment were tested including air channel size, shape, and inner diameter. The method of extruding alginate was also investigated and optimized for our application. By testing and optimizing these components, we were able to design a working prototype that enabled us to produce droplets and continue fine-tuning this technique.

Experimentation on the air flow rate and extrusion rate used during printing allowed us to optimize these parameters for ideal printing. The air needs to flow through the system at a minimum rate to produce small droplets, but this rate cannot be too high as to avoid major issues in droplet shape. The extrusion rate also needs to be above a minimum rate, in conjunction with the air flow speed. The finalized settings for these parameters were an air flow rate of 5 L/min and an extrusion rate of 0.07 mL/min.

Once air flow rate and extrusion rate were finalized, we tested other factors such as exposed needle length, alginate concentration, and calcium chloride concentration. We observed that too much exposed needle would result in poor shape and too little exposed needle would result in larger droplet shape. Of the three lengths tested (0.5mm, 1mm, and 1.5mm), we concluded that the middle length of 1mm was the optimal length for size and shape considerations. It was also concluded that the concentration of the alginate solution was an important factor, particularly with droplet shape. Low alginate concentration (1%) resulted in weak, nonuniform droplets while higher concentrations (1.5%, 2%) exhibited more spherical droplet shapes. The concentration of the solution used to crosslink the droplets was also examined. A weaker calcium chloride solution (50mM) likely increases time required for full crosslinking and therefore produces worse shape than a stronger solution (100mM). By combining all the factors mentioned, we were able to construct a viable droplet production technique that was used to produce mostly spherical droplets within our target size range of 200 – 400 μm.

4.1. Future Work

There are several areas of improvement that we would like to focus on in future works. For example, further optimization of the air-jet attachment could improve the longevity of individual attachments. Currently, the device is printed at the exact size to form an air-tight seal with the syringe to ensure air only escapes through the air channel. Over time, inserting and removing the syringe over and over wears down the inner wall of the attachment and can cause leaks. We would like to incorporate a rubber O-ring into this part of the design to allow for a tight seal without wearing down the inner wall. This

will allow us to use individual attachments for a longer period before they need to be replaced.

We could also adapt this attachment and technique back to a bioprinter, as was our original intention. This would only require some cosmetic changes to the attachment and an experimentation period to determine the optimal printing parameters. Reverting to an actual bioprinter would give the system XY printing capabilities, meaning we would be able to move the extrusion apparatus as it was producing droplets. This could be used for more complex printing, such as generating a rough number of droplets into each well of a 96-well plate.

Incorporating cells into the alginate bioink will likely change the properties of the solution, such as viscosity, which will impact how it behaves. This study has optimized parameters for printing with an alginate solution alone and will need to be reoptimized for the updated solution. The behavior of the alginate solution will also likely change based on the number of cells that are incorporated, i.e., the cell seeding density. Several exploratory experiments, like the air flow vs extrusion rate experiment in this paper, may be needed to determine the optimal parameters for droplet generation.

References

1. Tibbitt, M.W. and K.S. Anseth, *Hydrogels as extracellular matrix mimics for 3D cell culture.* Biotechnol Bioeng, 2009. **103**(4): p. 655-63.

2. Toh, W.S. and X.J. Loh, *Advances in hydrogel delivery systems for tissue regeneration.* Mater Sci Eng C Mater Biol Appl, 2014. **45**: p. 690-7.

3. Bochenek, M.A., et al., *Alginate encapsulation as long-term immune protection of allogeneic pancreatic islet cells transplanted into the omental bursa of macaques.* Nat Biomed Eng, 2018. **2**(11): p. 810-821.

4. Andersen, T., P. Auk-Emblem, and M. Dornish, *3D Cell Culture in Alginate Hydrogels.* Microarrays (Basel), 2015. **4**(2): p. 133-61.

5. Zhang, X., et al., *Analysis of regulatory network involved in mechanical induction of embryonic stem cell differentiation.* PLoS One, 2012. **7**(4): p. e35700.

6. Narasimhan, B.N., M.S. Horrocks, and J. Malmström, *Hydrogels with Tunable Physical Cues and Their Emerging Roles in Studies of Cellular Mechanotransduction.* Advanced NanoBiomed Research, 2021. **1**(10): p. 2100059.

7. Orr, A.W., et al., *Mechanisms of Mechanotransduction.* Developmental Cell, 2006. **10**(1): p. 11-20.

8. Lee, K.Y. and D.J. Mooney, *Alginate: properties and biomedical applications.* Prog Polym Sci, 2012. **37**(1): p. 106-126.

9. Candiello, J., et al., *Early differentiation patterning of mouse embryonic stem cells in response to variations in alginate substrate stiffness.* J Biol Eng, 2013. **7**(1): p. 9.

10. Martins, E., et al., *Oil encapsulation techniques using alginate as encapsulating agent: applications and drawbacks.* Journal of Microencapsulation, 2017. **34**(8): p. 754-771.

11. Paques, J.P., et al., *Preparation methods of alginate nanoparticles.* Advances in Colloid and Interface Science, 2014. **209**: p. 163-171.

12. Aguero, L., et al., *Functional role of crosslinking in alginate scaffold for drug delivery and tissue engineering: A review.* European Polymer Journal, 2021. **160**: p. 110807.

13. Richardson, T., P.N. Kumta, and I. Banerjee, *Alginate encapsulation of human embryonic stem cells to enhance directed differentiation to pancreatic islet-like cells.* Tissue Eng Part A, 2014. **20**(23-24): p. 3198-211.

14. Mitry, R.R., et al., *Alginate Encapsulation of Human Hepatocytes and Assessment of Microbeads.* Methods Mol Biol, 2017. **1506**: p. 273-281.

15. Bugarski, B., et al., *Electrostatic droplet generation: Mechanism of polymer droplet formation.* AIChE Journal, 1994. **40**(6): p. 1026-1031.

16. Wong, S.C., et al., *Flicking technique for microencapsulation of cells in calcium alginate leading to the microtissue formation.* J Microencapsul, 2016. **33**(2): p. 162-71.

17. Ciriza, J., et al., *Use of Flow Focusing Technique for Microencapsulation of Myoblasts*, in *Cell Microencapsulation: Methods and Protocols*, E.C. Opara, Editor. 2017, Springer New York: New York, NY. p. 207-216.

18. Wolters, G.H., et al., *A versatile alginate droplet generator applicable for microencapsulation of pancreatic islets.* J Appl Biomater, 1991. **3**(4): p. 281-6.

19. Gokhare, V.G., D. Raut, and D. Shinde, *A review paper on 3D-printing aspects and various processes used in the 3D-printing.* Int. J. Eng. Res. Technol, 2017. **6**(06): p. 953-958.

20. Lee, D., et al., *3D printed alginate bead generator for high-throughput cell culture.* Biomed Microdevices, 2021. **23**(2): p. 22.

21. Pal, V., et al., *High-throughput microgel biofabrication via air-assisted co-axial jetting for cell encapsulation, 3D bioprinting, and scaffolding applications.* Biofabrication, 2023. **15**(3).

22. Lee, B.-B., P. Ravindra, and E.-S. Chan, *Size and Shape of Calcium Alginate Beads Produced by Extrusion Dripping.* Chemical Engineering & Technology, 2013. **36**(10): p. 1627-1642.

23. Abdi, H. and L.J. Williams, *Tukey's honestly significant difference (HSD) test.* Encyclopedia of research design, 2010. **3**(1): p. 1-5.

Appendix

The following tables show data obtained from Tukey's tests in section 3.4.1. regarding the significant differences in droplet diameters between samples produced at different conditions. The value above each table represents the extrusion rate of all samples in the table.

0.05 mL/min

Condition Pairs		Mean Difference	MD Lower	MD Upper	p-value
3 L/min	4 L/min	231.02	249.88	268.74	0
3 L/min	5 L/min	338.85	352.06	365.28	0
3 L/min	6 L/min	402.76	415.73	428.7	0
4 L/min	5 L/min	86.259	102.18	118.11	1.0297E-31
4 L/min	6 L/min	150.13	165.85	181.57	0
5 L/min	6 L/min	55.54	63.668	71.796	0

0.09 mL/min

Condition Pairs		Mean Difference	MD Lower	MD Upper	p-value
3 L/min	4 L/min	211.74	223.71	235.68	0
3 L/min	5 L/min	246.03	257.81	269.58	0
3 L/min	6 L/min	295.9	308.16	320.43	0
4 L/min	5 L/min	27.261	34.097	40.933	0
4 L/min	6 L/min	76.808	84.456	92.104	0
5 L/min	6 L/min	43.018	50.359	57.7	0

0.11mL/min

Condition Pairs		Mean Difference	MD Lower	MD Upper	p-value
3 L/min	4 L/min	151.45	165.97	180.49	0
3 L/min	5 L/min	205.81	220.02	234.22	0
3 L/min	6 L/min	257.38	271.05	284.72	0
4 L/min	5 L/min	44.58	54.05	63.52	0
4 L/min	6 L/min	96.437	105.08	113.72	0
5 L/min	6 L/min	42.923	51.03	59.137	0